

1 **Estimating the depth and evolution of intrusions at resurgent** 2 **calderas: Los Humeros (Mexico)**

3 Stefano Urbani¹, Guido Giordano^{1,2}, Federico Lucci¹, Federico Rossetti¹, Valerio Acocella¹,
4 Gerardo Carrasco- Núñez³

5 ¹Dipartimento di Scienze, Università degli Studi Roma Tre, L.go S.L. Murialdo 1, I-00146 Rome, Italy

6 ²CNR - IDPA c/o Università degli Studi di Milano, Via Luigi Mangiagalli, 34, 20133 Milano

7 ³Centro de Geociencias, Universidad Nacional Autónoma de México, Campus UNAM Juriquilla, 76100, Queretaro,
8 Mexico

9 *Correspondence to:* Stefano Urbani (stefano.urban@uniroma3.it)

10 **Abstract.** Resurgent calderas represent a target with high potential for geothermal exploration, as they are associated
11 with the shallow emplacement of magma, resulting in a widespread and long lasting hydrothermal activity. Therefore,
12 evaluating the thermal potential of resurgent calderas may provide important insights for geothermal exploitation.
13 Resurgence is classically attributed to the uplift of a block or dome resulting from the inflation of the collapse-forming
14 magma chamber due to the intrusion of new magma. The Los Humeros volcanic complex (LHVC; Mexico), consisting
15 of two nested calderas (the outer Los Humeros and the inner, resurgent, Los Potrerros), represents an area of high
16 interest for geothermal exploration to optimize the current exploitation of the active geothermal field. Here we aim at
17 better define the characteristics of the resurgence in Los Potrerros, by integrating field work with analogue models,
18 evaluating the spatio-temporal evolution of the deformation and the depth and extent of the intrusions responsible for
19 the resurgence and which may represent also the local heat source(s).

20 Structural field analysis and geological mapping show that Los Potrerros area is characterized by several lava domes and
21 cryptodomes (with normal faulting at the top) that suggest multiple deformation sources localized in narrow areas.

22 The analogue experiments simulate the deformation pattern observed in the field, consisting of magma intrusions
23 pushing a domed area with apical depression. To define the possible depth of the intrusion responsible for the observed
24 surface deformations, we apply tested established relations for elliptical sources to our experiments with sub-circular
25 sources. We found that these relations are independent from the source and surface dome eccentricity and suggest that
26 the magmatic sources responsible for the deformation in Los Potrerros are present at very shallow depths (hundreds of
27 meters), which is in agreement with the well data and field observations. We therefore propose that the recent
28 deformation at LHVC is not a classical resurgence associated with the bulk inflation of a deep magma reservoir; rather
29 this is related to the ascent of shallow (<1 km) multiple magma bodies. A similar multiple source model of the
30 subsurface structure has been also proposed for other calderas with an active geothermal system (Usu volcano, Japan)
31 suggesting that the model proposed may have a wider applicability.

32 **1 Introduction**

33 Caldera resurgence consists of the post-collapse uplift of part of the caldera floor. Resurgence has been described in
34 several calderas worldwide (Smith and Bailey, 1968; Elston, 1984; Lipman, 1984 and references therein), representing a
35 frequent step in caldera evolution. Several mechanisms have been invoked to trigger resurgence, including the
36 pressurization of the hydrothermal system (Moretti et al., 2018), regional earthquakes (Walter et al., 2009), and
37 magmatic intrusion (Kennedy et al. 2012). Discriminating the contributions to the observed uplift of each of these
38 mechanisms is often challenging (Acocella, 2014). However, despite the possible hydrothermal and tectonic

39 contributions, field observations in eroded resurgent calderas (e.g. Tomochic, Swanson and McDowell, 1985; Kutcharo,
40 Goto and McPhie 2018; Turkey Creek, Du Bray and Pallister, 1999) coupled with the long timescale of the uplift of the
41 caldera floor (from tens to thousands years), suggest that the intrusion of magmatic bodies is the prevalent mechanism
42 for resurgence.

43 Resurgence is commonly attributed to the emplacement of silicic magmas at different depth levels under limited
44 viscosity contrasts with regard to the previously emplaced magma (Marsh, 1984; Galetto et al., 2017). However, though
45 rare, resurgence may be also triggered by the injection of more primitive magma (Morán-Zenteno et al., 2004; Kennedy
46 et al., 2012) or by the emplacement of basaltic sills, as recently documented at the Alcedo caldera (Galapagos; Galetto
47 et al., 2019). The shape of the intracaldera resurgent structures is variable, being characterized by elliptical domes with
48 longitudinal graben(s) at the top (e.g. Toba; De Silva et al., 2015; Snowdonia, Beavon, 1980; Timber Mountain,
49 Christiansen et al., 1977) or, less commonly, by sub-circular domes (e.g. Cerro Galan, Folkes et al., 2011; Long Valley,
50 Hildreth et al., 2017; Grizzly Peak, Fridrich et al., 1991) with both longitudinal grabens (Long Valley) or concentric
51 fault blocks (Grizzly Peak) at their top.

52 Whatever is the shape, resurgence is often associated with hydrothermal and ore forming processes, since the circulation
53 pattern and temperature gradients of geothermal fluids are structurally-controlled by the space-time distribution of faults
54 and fractures and by the depth and shape of the magmatic sources (e.g. Guillou Frottier et al., 2000; Prinbow et al.,
55 2003; Stix et al., 2003; Mueller et al., 2009). Therefore, the characterisation of the magma that drives resurgence
56 (location, depth and size) and of the factors controlling the release of the heat (permeability, fracture patterns, and fluid
57 flow) have important implications for the exploration and exploitation of renewable geothermal energy resources. In
58 particular, the estimation of the location, depth and geometry of the magmatic sources is crucial to define the
59 geothermal and mineral potential of resurgent calderas, allowing an economically sustainable exploration and
60 exploitation of their resulted natural resources.

61 The depth and size of the magmatic sources influences the deformation style of the resurgence at surface (Acocella et
62 al., 2001). Deep sources (i.e. depth/diameter ratio ~ 1 assuming a spherical source) are associated to resurgent blocks
63 (e.g. Ischia and Pantelleria, Acocella and Funicello, 1999; Catalano et al., 2009), whereas shallower sources (i.e.
64 depth/diameter ratio ~ 0.4) to resurgent domes (e.g. Valles and Yenkahe, Kennedy et al., 2012; Brothelande et al., 2016).
65 Moreover, uplift rates may change by one order of magnitude from ~ 1 to ~ 10 cm per year (e.g. Yellowstone and Iwo
66 Jima, Chang et al., 2007; Ueda et al., 2018). Nevertheless, despite showing different uplift styles and rates, these natural
67 examples share a common feature that is a coherent uplift of the caldera floor.

68 This scenario differs from the occurrence of deformation patterns characterized by the widespread and delocalized uplift
69 of several minor portions of the caldera floor, due to lava domes and/or cryptodomes, as observed at Usu volcano
70 (Japan, Matsumoto and Nakagawa, 2010; Tomya et al., 2010). A different depth and extent of the responsible source(s)
71 and, consequently, a different subsurface structure of the volcano is therefore suggested. A better assessment of the
72 subsurface structure in such cases has crucial implications for geothermal exploration in order to maximize the
73 geothermal production.

74 The Los Humeros Volcanic Complex (LHVC, Mexico) is an important geothermal target area, consisting of two nested
75 calderas: Los Humeros (the outer, larger and older one) and Los Potreros (the inner, smaller and younger one) (Fig. 1).
76 The latter is characterized by the resurgence of its floor, which was previously interpreted as due to uplift processes
77 related to the inflation of a several km deep magma chamber (Norini et al., 2015, 2019).

78 This paper aims at (1) evaluating the depth of the intrusion(s) responsible for the uplift in the LHVC area; (2) explain
79 the spatio-temporal evolution of the observed deformation of the caldera floor and (3) test the validity of the linear

80 relationship between the surface deformation structures and depth of elliptical sources (Brothelande and Merle 2015)
81 for sub-circular sources. To achieve these goals, we integrate results from structural field investigations carried out
82 within the Los Potreros caldera with those derived from analogue experiments specifically designed to constrain the
83 depth of the deformation source(s) in volcanic caldera environments. The obtained results show that: (1) the relation
84 between the source depth and surface deformation structures is independent from the source eccentricity; (2) the LHVC
85 is characterized by discontinuous and small-scale (areal extent $\sim 1 \text{ km}^2$) surface deformations generated from multiple
86 and shallow-emplaced ($< 1 \text{ km}$ depth) magmatic bodies. These results should be taken into account for the planning of
87 future geothermal operations at the LHVC and in other calderas showing similar surface deformation.

88 **2 Geological-structural setting**

89 LHVC is located at the eastern termination of the Trans Mexican Volcanic Belt (TMVB, see inset in Fig. 1). The TMVB
90 is the largest Neogene volcanic arc in Mexico ($\sim 1000 \text{ km}$ long and up to $\sim 300 \text{ km}$ wide), commonly associated with the
91 subduction of the Cocos and Rivera plates beneath the North American plate along the Middle American trench (Ferrari
92 et al., 2012, and references therein). The LHVC consists of two nested calderas formed during the Pleistocene: the outer
93 $18 \times 16 \text{ km}$ Los Humeros caldera and the inner $10 \times 8 \text{ km}$ Los Potreros caldera (Fig. 1, Ferriz and Mahood, 1984;
94 Norini et al., 2015; Carrasco-Núñez et al., 2017b).

95 Based on updated stratigraphic and geochronological information, the evolution of the LHVC can be divided into three
96 main eruptive stages (Table 1, Carrasco-Núñez et al., 2017b, 2018). Pre-caldera volcanism extended between ca. 700
97 and 164 ka (U-Th and $^{39}\text{Ar}/^{40}\text{Ar}$ datings in Carrasco-Núñez et al., 2018), showing evidence for an extended building
98 phase leading to the establishment of the large volume rhyolitic reservoir, which fed several lava domes erupted to the
99 western border of the Los Humeros Caldera. A Caldera stage started at ca. 164 ka (U-Th and $^{39}\text{Ar}/^{40}\text{Ar}$ ages, Carrasco-
100 Núñez et al., 2018), with the eruption of the 115 km^3 Xaltipan ignimbrite that triggered the collapse of the Los Humeros
101 caldera. This was followed by a Plinian eruptive episodic sequence, characterized by the emplacement of several
102 rhyodacitic pumice fallout layers grouped as the Faby Tuff (Ferriz and Mahood, 1984). The Caldera stage ended with
103 the eruption of the 15 km^3 Zaragoza rhyodacite-andesite ignimbrite at $69 \pm 16 \text{ ka}$ ($^{39}\text{Ar}/^{40}\text{Ar}$ ages, Carrasco-Núñez et al.,
104 2018) associated with the collapse of the nested Los Potreros caldera.

105 A post-caldera stage ($< 69 \text{ ka}$) is interpreted by Carrasco-Núñez et al. (2018) as composed by two main eruptive phases:
106 (i) a late Pleistocene resurgent phase, characterized by the emplacement of silica-rich small domes and disperse
107 explosive activity within Los Potreros caldera, followed by (ii) Holocene basaltic to trachytic monogenetic, intra-
108 caldera and at the caldera-rim, volcanism. This eruptive behaviour indicates a change in the configuration of the
109 magmatic plumbing system with respect to the early caldera stage of Los Humeros, which has been referred to an
110 unique, large and homogenized magma reservoir (e.g. Ferriz and Mahood, 1984; Verma, 1985). It is instead in favour of
111 a heterogeneous multi-layered system vertically distributed in the crust, with a deep (ca. 30 km depth) basaltic reservoir
112 feeding progressively shallower and smaller distinct stagnation layers, pockets and batches up to very shallow
113 conditions (ca. 3km) (Lucci et al., under review).

114 During the early resurgent phase of the post-caldera stage, rhyolitic domes were emplaced along the northern rim of the
115 Los Humeros caldera and within the caldera at $44.8 \pm 1.7 \text{ ka}$ (U-Th ages) and $50.7 \pm 4.4 \text{ ka}$ ($^{39}\text{Ar}/^{40}\text{Ar}$ ages), respectively
116 (Carrasco-Núñez et al., 2018). This effusive activity was followed by several explosive eruptions, which originated a
117 dacitic air fall called Xoxoctic Tuff (0.6 km^3 , Ferriz and Mahood, 1984) and a pyroclastic sequence that includes an
118 explosive breccia and pyroclastic flow deposits comprising the Llano Tuff (Ferriz and Mahood 1984; Willcox, 2011).

119 The Holocene ring-fractures fed bimodal magmatism characterized by both explosive and effusive activity, producing
120 several lava flows and domes, as well as the the ca. 7 ka (C-14 age, Dávila-Harris and Carrasco-Núñez, 2014) Cuicuiltic
121 Member during periods of dominant explosive activity. It consists of alternating pumices and scoriae erupted during
122 contemporaneous sub-Plinian to Strombolian activity from multiple vents located mostly along the inner part of the
123 caldera and outer caldera ring faults (Dávila-Harris and Carrasco-Núñez, 2014). During this phase, less evolved lavas
124 (trachyandesite to basalt) were erupted within and outside Los Humeros caldera, including the olivine-bearing basaltic
125 lava that fills the previously formed Xalapasco crater (Fig. 1). Trachytic lava flows are the most recent activity recorded
126 in the area, with an age of ca. 2.8 ka (C-14 age, Carrasco-Núñez et al., 2017b).

127 The reconstruction of the shallow stratigraphy within Los Potreros caldera is chiefly derived from the analysis of
128 available well-logs (Figs. 2a-b Carrasco-Núñez et al., 2017a, b). Overall, the post-caldera units are lithologically
129 dominated by lava flows resting on ignimbrite deposits emplaced during caldera stage. Ignimbrites of the caldera stage
130 rest in turn on a thick sequence dominated by andesite lavas dated at ca. 1.4-2.8 Ma ($^{39}\text{Ar}/^{40}\text{Ar}$ ages, Carrasco-Núñez et
131 al., 2017a). The subsurface geometry of the pre- and syn-caldera products is shown in Figs. 2a-b, where the in-depth
132 geometry of the different magmatic products are cross-correlated and projected along the N-S and E-W direction,
133 respectively. The N-S projection shows a constant depth of the top surface of the pre-caldera andesites that is associated
134 with a highly variable depth (down to -400 m) of the top surface of the syn-caldera Xaltipan ignimbrite. The W-E
135 projection shows a higher depth variability of both the top surface of the pre-caldera group (down to -500 m between H-
136 19 and H-25 wells) and that of the Xaltipan ignimbrite (down to -400 m between H-19 and H-10 wells). Basaltic and
137 rhyolitic-dacitic lavas occur at various depths (Carrasco-Núñez et al., 2017a); rhyolites-dacites are located mostly at the
138 base (H-20 and H-26 wells) or within (H-05 well) the caldera group or the old andesite sequence (H-25 and H-19
139 wells). Basalts are located only within the pre-caldera andesite sequence, both at its base (in contact with the limestone
140 basement; H-5 and H-8 wells) and at its top (in contact with the base of the caldera sequence; H-10 well). These
141 bimodal lava products, showing an irregular lateral distribution, have been interpreted as subaerial (Carrasco-Núñez et
142 al., 2017a).

143 The structural architecture of the LHVC is controlled by a network of active extensional fault systems, made of NNW-
144 SSE, N-S, NE-SW and E-W striking fault strands cutting across the Los Potreros caldera floor. The following main
145 faults were recognised (Norini et al., 2015, 2019; Calcagno et al., 2018) (Fig.1): (i) Maxtaloya (NNW-SSE striking), (ii)
146 Los Humeros and Loma Blanca (N-S striking), (iii) Arroyo Grande (NE-SW striking), (iv) Las Viboras and Las Papas
147 (E-W striking). Such active fault systems are interpreted as due to the recent/active resurgence of the Los Potreros
148 Caldera. Since the faults do not show continuity beyond the caldera border, their scarps decrease in height towards the
149 periphery of the caldera and the dip-slip displacement vectors show a semi-radial pattern (Norini et al., 2015).

150 The source of the areal uplift has been inferred to be the inflation of a saucer or cup shaped deep magmatic source
151 elongated NNW-SSE, up warping a 8 x 4 km resurgent block, centred in the SE portion of the caldera, delimited to the
152 W by the NNW-SSE main faults, and toward the north, east and south by the caldera rim (Fig.1, Norini et al., 2015,
153 2019).

154 The seismic activity between 1994-2017 is clustered along the Loma Blanca, Los Humeros and Arroyo Grande faults
155 (Lermo et al., 2018; Fig. 1). Most of the earthquakes show a magnitude (M_w) between 1 and 2.5 and have been mainly
156 interpreted as induced by the geothermal exploitation activity (injection of fluids and hydrofracturing; Lermo et al.,
157 2018). Four major earthquakes ($M_w= 3.2, 3.6, 3.9$ and 4.2 , at a depth of 1, 4, 2.2 and 1.8 km, respectively) have also
158 been reported, with focal depths close to the trace of the active faults (Loma Blanca and Los Humeros, Fig.1). Such

159 major earthquakes have been interpreted as triggered by fault reactivation due to fluid/brine circulation injected from
160 geothermal wells (Lermo et al., 2018).

161 **3 Methods**

162 The scientific rationale adopted in this study is based on structural field work combined with analogue models aimed to
163 constrain the depth of the deformation sources in the caldera domain. We also tested if the relation that constrains the
164 depth of the source deformation from surface parameters adopting elliptical sources (Brothelande and Merle 2015) is
165 verified also for sub-circular sources.

166 **3.1 Structural field work**

167 Structural field work was carried out on the post-caldera (late Pleistocene to Holocene) deposits to characterise the
168 surface deformation related to the recent activity of the Los Potreros caldera and constrain the morphotectonic
169 fingerprints of the resurgence to evaluate its source and areal extent. The geometry and distribution of the observable
170 faults and joints were defined at the outcrop scale by measuring their attitudes (strike and dip; right-hand rule) and
171 spacing. Fault kinematics was assessed through classical criteria on slickensides fault surfaces, such as Riedel shears,
172 growth fibers and sheltering trails (Doblas, 1998). The published geological map (Carrasco-Núñez et al., 2017b) and
173 geothermal well data has been used (Carrasco-Núñez et al., 2017a) to correlate the surface structures at a broader scale.
174

175 **3.2 Analogue models: experimental set-up and scaling**

176 Five experiments were undertaken simulating the ascent of a viscous sub-circular intrusion in a brittle overburden to test
177 the validity of existing relationships between the depth of elliptical intrusions and the observed surface deformation
178 (Brothelande and Merle, 2015). The experimental set-up (Fig. 3) consists of a 31×31 cm glass box filled with a sand
179 pack (crust analogue) of variable thickness (T , of 10, 30 and 50 mm, respectively). In each experiment we imposed a
180 layering using a non-cohesive marine sand below a layer of crushed silica sand (grain size = 40-200 μm , cohesion = 300
181 Pa), fixing the thickness ratio of the two layers (T_u/T_1) to 1, to simulate the stratigraphy in Los Potreros (stiffer post
182 caldera lava flows above softer and less cohesive ignimbrite deposits emplaced during the caldera collapse stage). At
183 the base of the sand pack, a piston, controlled by a motor, pushes upward the silicone (magma analogue) placed inside a
184 cylinder 8 cm in diameter. The injection rate is fixed for all the experiments to 2 mm/hr and each experiment was
185 stopped at the onset of the silicone extrusion. Both sand and silicone physical properties are listed in Table 2.

186 At the end of each experiment, the surface has been covered with sand to preserve their final topography and were
187 wetted with water for cutting in sections to appreciate the subsurface deformation. Such sections were used to measure
188 the mean dip of the apical depression faults (θ) induced by the rising silicone. A digital camera monitored the top view
189 deformation of each experiment at 0.02 fps and a laser scanner, placed next to the camera, provided high-resolution data
190 (maximum error ± 0.5 mm) of the vertical displacement that was used to measure in detail the geometrical features of
191 the deformation i.e. dome diameter (L_d), apical depression width (L_g) and dome flank mean dip (α). According to the
192 Buckingham- Π theorem (Merle and Borgia 1996 and references therein), our models need 7 independent dimensionless
193 numbers to be properly scaled (i.e. 10 variables minus three dimensions; Table 2). Such dimensionless numbers can be
194 defined as the ratios (Π) listed in Table 3. Some values of Π_5 , representing the ratio between the inertial and viscous
195 forces, are very small both in nature and experiments (1.3×10^{-20} and 6.1×10^{-10} , respectively), indicating that the
196 inertial forces are negligible with respect to the viscous forces in both cases.

197 **4 Results**

198 **4.1 Structural geology**

199 The outcropping post-caldera lithologies within the Los Potreros Caldera consist of: (1) the Cuicuiltic Member, which
200 blankets most of the surface of the upper half of the studied area; (2) basaltic lava flows filling the Xalapasco crater and
201 the NW portion of the caldera; and (3) trachyandesitic and trachytic lava domes and thick flows extending in the
202 southern half of the caldera and rhyolitic domes in its central part (Fig. 4). Field work documented that the more
203 evolved lavas form five nearly N-S trending elliptical domes, distributed in both sides of the Los Humeros Fault (Figs. 4
204 and 5a): (i) a 2 km long \times 1.2 km wide trachytic dome located to the west of the Maxtaloya and Los Humeros faults, (ii)
205 a 1 \times 0.7 km trachyandesitic dome located in a northeast area of the Maxtaloya fault, and (iii) one trachyandesitic and
206 two obsidian smaller domes (0.4 \times 0.2 km) to the eastern side of the Los Humeros Fault (LH-11 in Fig. 4).

207 Field work concentrated on the three main uplifted areas corresponding to the surface expression of the Loma Blanca,
208 Arroyo Grande and Los Humeros faults (labelled LH1-2, LH9 and LH10 respectively in Fig. 4). The observed
209 structures in these uplifted areas (joints and faults) affect the deposits of the post-caldera phase. Based on field
210 evidence, we also propose a revised interpretation of the surface structures identified by previous studies (Norini et al.,
211 2015, 2019), distinguishing between lineaments (morphological linear scarps, with no measurable fault offsets and/or
212 alteration at the outcrop scale), active and inactive faults, instead associated with measurable fault offsets and with
213 active or fossil alteration, respectively (Fig. 4). We present below a description of the structures mapped in the studied
214 area, highlighting their temporal and spatial relationships with the post-caldera geological formations. We identified two
215 inactive faults (Maxtaloya and Arroyo Grande), a morphological lineament (Las Papas) and two currently active faults
216 (Los Humeros and Loma Blanca).

217 **4.1.1 Las Papas lineament (sites LH-07, LH-08)**

218 The E-W trending Las Papas lineament is localised within the Cuicuiltic Member (LH-07; Fig. 5b). We identified an
219 erosional surface along the scarp, where unaltered and undeformed Cuicuiltic Member rocks rest above the Xoxoctic
220 Tuff (LH-08, Fig. 5c). The E-W trending morphological lineament of Las Papas is probably due to differential erosion
221 of the softer layers of the pyroclastic deposits, successively blanketed by the Cuicuiltic Member.

222 **4.1.2 Arroyo Grande (site LH-09) and Maxtaloya scarps**

223 The NE-SW Arroyo Grande scarp (Fig. 6a) exposes strongly altered and faulted (NW striking faults, mean attitude
224 N144°/68°, number of data (n) = 8) lavas and ignimbrites unconformably covered by the unaltered Cuicuiltic Member
225 (Fig. 6b). The offset observed at the outcrop-scale for the single fault strands is ca. 0.5 m, with a dominant normal dip-
226 slip kinematics (pitch angle of the slickenlines ranging 99°-106°). The inferred cumulative displacement at Arroyo
227 Grande is \sim 10 m. Similarly, an outcrop on the Maxtaloya scarp (in front of well H-6) shows altered trachyandesites
228 covered by unaltered Cuicuiltic Member rocks (Fig. 6c).

229 **4.1.3 Los Humeros (site LH-10)**

230 The fault scarp of the N-S striking (mean attitude N174°/73°, n = 8) Los Humeros Fault exposes the altered portions of
231 the Cuicuiltic Member. Fault population analysis reveals a dominant normal dip-slip (mean pitch angle of the
232 slickenlines: 84°) kinematics, as documented by both Riedel shears and carbonate-quartz growth steps. The main fault
233 surface is sutured by a trachyandesitic extrusion (Fig. 6d), localised along an aligned N-S dome (site LH-11 in Fig. 4).

234 Moreover, ~150 m southward from the outcrop of the fault scarp, a 5×3 m wide trachyandesitic plug shows vertical
235 striation on its surface due to a subsurface vertical flow of the trachyandesite (Fig. 6e). The observed displacement at
236 the outcrop scale, as indicated by the height of the fault scarp, is ~ 10 m.

237 **4.1.4 Loma Blanca (LH-01, LH-02)**

238 The Loma Blanca Fault system (sites LH-01 and LH-02) is located in an active degassing area, where faults and
239 fractures are frequent. The fault system is on top of an elongated crest (within an apical depression) of a morphological
240 bulge, ~ 1 km in width and 30 m in height. At this location, the Cuicuiltic Member and the underlying trachyandesite
241 lavas are strongly altered (Fig. 6f). Evidence of stockwork veining and diffuse fracturing of the lavas suggests
242 hydrofracturing and structurally controlled fluid flow and alteration. A set of NNE-SSW striking conjugate extensional
243 faulting and jointing (joint spacing ~0.5 m) is observed. The faults (mean attitude $N26^{\circ}/71^{\circ}$, $n= 6$) show a normal dip-
244 slip kinematics (pitch of the slickenlines ranging 82° - 104°). Joint systems found in the Cuicuiltic Member strike sub-
245 parallel to the faults (mean attitude $N37^{\circ}/72^{\circ}$, $n= 14$). The inferred cumulative displacement of the faults, estimated by
246 the depth of the apical depression, is ~ 5 m.

247 In summary, the 22 mapped faults in all the structural outcrops of the area show a main NNW-SSE strike (Fig. 6g) with
248 a dominant dip slip movement (mean pitch angle of slickenlines 88° , $n= 16$) which is sub-parallel to the N-S elongation
249 of the lava domes and the Xalapasco crater.

250 **4.2 Experimental results**

251 Here we show three representative experiments with increasing overburden thickness (experiments 1-3-5 with $T= 10$,
252 30 and 50 mm). Table 4 shows the measured parameters in the experiments. Some experiments (1-2 and 3-4) were
253 replicated with the same imposed boundary conditions and show the same result, which ensures model reproducibility.

254 Overall, the experiments show a similar deformation pattern: a first stage characterized by the uplift of a sub-circular
255 dome, bordered by inward dipping reverse faults, and a second stage characterized by the subsidence of the apical part
256 of the dome where normal faulting occurs (apical depression formation Fig. 7a-i). The reverse and normal faults are ring
257 faults and are associated with the formation of radial fractures from the dome centre. A different shape of the apical
258 depression is observed with $T/D > 0.12$. In exp.1 ($T/D = 0.12$) an annular peripheral depression formed as the silicone
259 reached the surface at the edge of the cylinder (Fig.7c). Conversely, in exp. 3 and 5 ($T/D= 0.37$ and 0.63 respectively) a
260 sub-circular apical depression formed as the silicone reached the surface at the centre of the dome (Fig.7g, m).

261 Despite the T/D ratio, all the experiments show that both the dome diameter and apical depression width increase
262 linearly with the overburden thickness (ranging from 105 to 164 mm and from 14 to 58 mm respectively, Table 4,
263 Fig.8). The dome diameter increases abruptly with time, becoming almost constant at an early stage of the experiment
264 (Fig.9a); the apical depression width shows a similar pattern even if it enlarges slightly with time (after the first abrupt
265 increase) as the silicone rises towards the surface (Fig. 9b), suggesting that the intrusion depth has an higher influence
266 on the apical depression width, in agreement with Brothelande and Merle (2015).

267

268 **5. Discussion**

269 **5.1 Interpretation of the analogue experiments**

270 The deformation pattern observed in the analogue experiments for thicker overburdens (experiments 3-4 and 5 with
271 $T/D= 0.37$ and 0.63), showing a sub-circular dome and an apical depression, is in agreement with previous analogue
272 experimental results (Acocella et al., 2001; Marti et al. 1994; Walter and Troll 2001). However, for thinner overburdens

273 (exps. 1-2, $T/D= 0.12$), we observed a new deformation pattern at the surface consisting of an annular peripheral
274 depression due to the rising of the silicone at the edge of the cylinder rather than its centre. We infer that in these
275 experiments, since the rising silicone was very close to the surface, the sagging of the sand overburden pushed
276 downward the centre of the silicone that squeezed up at the edges of the cylinder. Such process may also explain the
277 two linear grabens that formed in the experiments with elliptical sources for small overburden thicknesses (ratio $T/D \sim$
278 0.1 , Brothelande and Merle 2015).

279 The deformation pattern observed in our experiments is independent with respect to the imposed strain (i.e. uplift) rate
280 or the viscosity of the intruding material as suggested by the similarity with results obtained in previous studies with
281 higher strain rates (Acocella and Mulugeta, 2002) or lower viscosity intruding materials (Galletto et al., 2017; Marti et
282 al. 1994; Walter and Troll, 2001). On the other hand, the occurrence of an apical depression is dependent on the
283 thickness (i.e. depth) of the intrusion since thin intrusions relative to their depths will generate sub-circular domes
284 without any apical depression (Galland et al., 2009; Galland, 2012). Moreover, our results confirm that the apical
285 depression width shows a linear correlation with the source depth (Fig. 8) as estimated in Brothelande and Merle (2015)
286 for elongated sources. This evidence documents that such relation is independent from the source eccentricity or shape
287 of the extensional structures at the top of the dome (i.e. linear graben or sub-circular depression) suggesting that any
288 elongation of the surface structure represents only a minor complication of the basic deformation pattern as already
289 pointed out by (Roche et al., 2000).

290

291 **5.2 Origin and extent of the resurgence in the LHVC**

292 The distribution of the alteration patterns and deformation characteristics of the post caldera deposits can be used to
293 infer the origin and extent of the uplift within the LHVC. In particular, whether the 7.4 ka Cuicuiltic Member was
294 involved in the deformation and alteration allow constraining the spatio-temporal evolution of the surficial deformation
295 and associated uplifts in Los Potreros. Unaltered and undeformed deposits of the Cuicuiltic Member crop out along the
296 E-W Las Papas lineament and unconformably cover altered and faulted lavas and ignimbrites along the Arroyo Grande
297 and Maxtaloya scarps. Alteration and deformation of the Cuicuiltic Member occurs along the Los Humeros Fault scarp
298 and within the apical depression of the Loma Blanca bulge. The vertical striations of the trachyandesitic plug near the
299 Los Humeros fault scarp suggest that the ascent of the plug induced the uplift, the normal dip-slip faulting and alteration
300 of the Cuicuiltic Member.

301 The observations suggest that Los Potreros is not a classic resurgent caldera (i.e. a caldera characterised by a large-scale
302 process localized in a single area) but is characterised by a discontinuous uplift process in space and time, inducing
303 small-scale deformations at each pulse (Fig. 10a-d). In particular, it was active in the south and north-eastern sector of
304 the caldera, at Maxtaloya and Arroyo Grande (Fig. 10a), prior to the deposition of the Cuicuiltic Member (~ 7.4 ka),
305 and then moved towards N along the Los Humeros and Loma Blanca scarps during and post the eruption of the
306 Cuicuiltic Member (Fig. 10b-d). The felsic lava found at the Los Humeros Fault scarp shows a similar mineral
307 assemblage to the felsic domes located further south (Fig. 4); thus, the Los Humeros scarp may represent the final stage
308 (i.e. effusive eruption of felsic magmas, (Fig. 10c) of the uplift process, which is thus driven by the ascent of relatively
309 narrow (hundreds of meters) and highly viscous felsic magma batches. This is supported by the N-S elongation of the
310 identified lava domes which is sub-parallel to the orientation of the measured fault planes (NNW-SSE), indicating that
311 the observed deformation is closely related to the post-caldera volcanism. The ascent of such magma bodies is inferred
312 here to drive the recent uplift and deformation of the Loma Blanca bulge, as suggested by the active fumaroles and
313 extensive alteration of both the Cuicuiltic Member and post-caldera lavas (Fig. 10d). The presence of such shallow

314 magma bodies is also suggested by the four major earthquakes recorded in Los Potreros, which have been previously
315 interpreted to be induced by geothermal exploitation (Lermo et al., 2018). However, since the magnitude of the seismic
316 events induced by geothermal exploitation activities is usually lower (i.e. < 3, Evans et al., 2012 and references therein),
317 the higher magnitude (between 3.2 and 4.2) of the earthquakes in Los Potreros suggests that they may be more likely of
318 volcano-tectonic origin due to shallow magma emplacement.

319 To further support the above interpretation from field observations, results from the presented analogue models were
320 used to constrain the magma source depth from the geometrical parameters measured in the experiments (L_g , θ , α , Table
321 4). We calculated the theoretical overburden thickness (i.e. the intrusion depth, T_t , Table 4) as follow (Brothelande and
322 Merle, 2015):

$$323 \quad T_t = \frac{1}{2} L_g \times \frac{\sin(\theta + \alpha)}{\cos \theta} \quad (1)$$

324 Comparing the percentage difference (σ) between the imposed experimental (T) and theoretical (T_t) overburden
325 thickness values, we calculate the associated error in the evaluation of the intrusion depth in the models (σ , Table 4,
326 Fig.8). We then use equation (1) for the evaluation of the heat source depth at the Loma Blanca bulge considering $\sigma \sim$
327 40 % (maximum value of the experiments excluding those showing an annular depression that was not observed in the
328 field). For the Loma Blanca bulge $L_g = 286$ m, $\theta = 71^\circ$, $\alpha = 4.5^\circ$, the estimated intrusion depth is 425 ± 170 m. Such
329 relatively shallow depth is within the range of depths of rhyolitic-dacitic domes drilled in geothermal wells (spanning
330 from 300 to 1700 m, Fig. 2a-b) and is consistent with the hypothesis that the uplift is driven by small and delocalized
331 magmatic intrusions, as suggested by the field data.

332 The rhyolites-dacites have been previously interpreted of subaerial origin (Carrasco-Núñez et al., 2017a), but we
333 suggest that at least some of them can be reinterpreted as intrusions of felsic cryptodomes based on the following
334 considerations: (i) the occurrence of rhyolite-dacite lava bodies within the thick pre-caldera old andesite sequence is
335 unusual and does not have a subaerial counterpart; (ii) the rhyolite body in well H-20 (Fig. 2b) up warps both the
336 intracaldera ignimbrite sequence and the post-caldera lavas (showing a reduced thickness) indicating that the caldera
337 forming ignimbrites do not level out the paleo-topography; and (iii) the top of the Xaltipan ignimbrite shows an higher
338 depth variation than the pre caldera andesite (Fig. 2a) highlighting a local and discontinuous uplifting of the Xaltipan
339 ignimbrite. Such evidence can be more easily reconciled with the intrusion of felsic cryptodomes within the volcanic
340 sequence, rather than with a regular layer-cake stratigraphy.

341

342 **5.3 Implications for the structure of the LHVC geothermal field**

343 The combination of field and modelling data support that the uplift in Los Potreros caldera is due to multiple
344 deformation sources in narrow areas that do not represent resurgence *sensu stricto*. Such localized recent deformation
345 within Los Potreros caldera appears to be linked to small magmatic intrusions located at relatively shallow depths (i.e. <
346 1 km) as in Loma Blanca, where the estimated intrusion depth calculated from the experimental data is 425 ± 170 m.

347 This model differs from the general accepted idea of resurgence in Los Potreros induced by the inflation of a saucer or
348 cup shaped deep magmatic intrusion (Norini et al., 2015, 2019). The resurgence is inferred to be centred beneath the
349 sector of the caldera traversed by the E-W lineaments and limited by the Maxtaloya and Arroyo Grande faults (sector S1
350 in Norini et al., 2015). The thermal anomalies identified by Norini et al. (2015) show that the temperatures are
351 unexpectedly cold beneath the inferred centre of the resurgent block, where the highest temperatures should be
352 expected. By contrast, sharp and narrow temperature peaks, spatially coincident with Los Humeros and Loma Blanca
353 faults, are consistent with the presence of shallow and delocalized heat sources. Indeed, the inflation of the deep magma
354 chamber of the LHVC, inferred to be at 5 to 7-8 km of depth (Verma, 1983, 2000, 2011) and extending 9 km in radius

355 and 6 km in length (thus coinciding with the Los Humeros caldera rim, Verma et al., 1990), should have resulted in a
356 much wider uplift and with higher magnitude than the one observed in the field. Resurgence resulting from magma
357 remobilization of the deep chamber that produced collapse is characterized by a larger-scale surface deformation
358 (thousands of meters of uplift extending for tens of kilometers on the surface) as shown in many large calderas
359 worldwide (Toba, de Silva et al., 2015; Cerro Galan, Folkes et al., 2011; Ischia, Carlino, 2012).

360 It is therefore unlikely that the replenishment of new magma in the caldera forming deep magma chamber accounts for
361 the magnitude (few tens of meters) and discontinuous spatial distribution of the deformation in Los Potreros.

362 Such a model of the recent uplifting in Los Potreros is supported by field-based petrographic-mineralogical analysis
363 showing that the present-day magmatic plumbing system is characterized by multiple magma levels spanning from a
364 deep (30-33 km) basaltic reservoir to very shallow (~ 1.5 km), smaller, trachyandesitic-trachytic magma batches (Lucci
365 et al., under review).

366 A similar model of the plumbing system has been proposed to explain the eruptive activity of Usu volcano (Japan) since
367 1663, a post caldera cone of the Toya caldera consisting of a basaltic main edifice surmounted by 3 felsic lava domes
368 and more than 10 cryptodomes. Petrochemical data at Usu suggest the presence of multiple magma batches (i.e. sills) at
369 0.25-2 km deep that originated from partial melting of a metagabbro (Matsumoto and Nakagawa, 2010; Tomya et al.,
370 2010).

371 Our proposed model has implications for planning future geothermal exploration: siting of future geothermal wells
372 should consider that the presence of shallow heat sources within the caldera may complicate the pattern of isotherms
373 associated with the deeper heat flow.

374 **6 Conclusions**

375 By integrating field work with analogue models, we constrain the late Pleistocene-Holocene spatio-temporal evolution
376 of volcanism of the LHVC and estimate the depth of the magmatic intrusions feeding the active geothermal system.
377 New findings on experimental analogue models of resurgent domes are also provided.

378 These are the main results that can be extracted from this study:

- 379 1. The distribution of the alteration patterns and deformation of the Cuicuiltic Member suggests that the recent (post-
380 caldera collapse) uplift in Los Potreros caldera moved progressively northwards, from the south and north-eastern
381 sector of the caldera towards N along the Los Humeros and Loma Blanca scarps.
- 382 2. The estimated depth of the intrusions responsible for such uplift is very shallow, as calculated from the experimental
383 data for the Loma Blanca bulge (425 ± 170 m).
- 384 3. The recent uplift in Los Potreros is discontinuous in space and time, inducing small-scale (areal extent ~ 1 km²)
385 deformations originating from multiple and shallow (< 1 km depth) magmatic bodies, thus not representing a classic
386 resurgent caldera, which usually involves large scale deformation (areal extent of several km²).
- 387 4. The relation that relates the magmatic source depth with the surface parameters of resurgent domes is independent by
388 the source eccentricity, similarly to what already verified for sub-circular intrusions.

390 **Acknowledgements**

391 CFE is kindly acknowledged for allowing work on the Los Humeros geothermal field. Federico Galetto helped for laser
392 scanner data processing. Fabio Corbi and Matteo Trolese provided technical support in building the experimental set-up.
393 Gianluca Norini is acknowledged for logistic support in the field. Alessandra Pensa kindly helped with figure drawings.
394 Funded by the European Union's Horizon 2020 GEMex Project (grant agreement No. 727550) and by the Mexican

395 Energy Sustainability Fund CONACYT-SENER, WP 4.5 of the Project 2015-04-268074. More information can be
396 found on the GEMex Website: <http://www.gemex-h2020.eu>. The Grant to Department of Science, Roma Tre University
397 (MIUR-Italy Dipartimenti di Eccellenza, ARTICOLO 1, COMMI 314 – 337 LEGGE 232/2016) is gratefully
398 acknowledged.

399

400 References

401 Acocella, V.: Great challenges in volcanology: how does the volcano factory work?, *Front. Earth Sci.*, 2:4,
402 <https://doi.org/10.3389/feart.2014.00004>, 2014.

403 Acocella, V., and Funicello, R.: The interaction between regional and local tectonics during resurgent doming: the case
404 of the island of Ischia, Italy, *J. Volcanol. Geoth. Res.*, 88, 109-123, [https://doi.org/10.1016/S0377-0273\(98\)00109-7](https://doi.org/10.1016/S0377-0273(98)00109-7),
405 1999.

406 Acocella, V., and Mulugeta, G.: Experiments simulating surface deformation induced by pluton emplacement,
407 *Tectonophysics*, 352, 275-293, [https://doi.org/10.1016/S0040-1951\(02\)00218-4](https://doi.org/10.1016/S0040-1951(02)00218-4), 2002.

408 Acocella, V., Cifelli, F., and Funicello, R.: The control of overburden thickness on resurgent domes, *J. Volcanol. Geoth.*
409 *Res.*, 111, 137–153, [https://doi.org/10.1016/S0377-0273\(01\)00224-4](https://doi.org/10.1016/S0377-0273(01)00224-4), 2001.

410 Arellano, V.M., García, A., Barragán, R.M., Izquierdo, G., Aragón, A., and Nieva, D.: An updated conceptual model of
411 the Los Humeros geothermal reservoir (Mexico), *J. Volcanol. Geoth. Res.*, 124, 67–88, [https://doi.org/10.1016/S0377-0273\(03\)00045-3](https://doi.org/10.1016/S0377-0273(03)00045-3), 2003.

413 Beavon, R.V.: A resurgent cauldron in the early Paleozoic of Wales, U.K., *J. Volcanol. Geoth. Res.*, 7, 157-174,
414 [https://doi.org/10.1016/0377-0273\(80\)90025-6](https://doi.org/10.1016/0377-0273(80)90025-6), 1980.

415 Brothelande, E., Peltier, A., Got, J.L., Merle, O., Lardy, M., and Garaebiti, E.: Constraints on the source of resurgent
416 doming inferred from analogue and numerical modeling — Implications on the current feeding system of the Yenkahe
417 dome–Yasur volcano complex (Vanuatu), *J. Volcanol. Geoth. Res.*, 322, 225–240,
418 <https://doi.org/10.1016/j.jvolgeores.2015.11.023>, 2016.

419 Brothelande, E., and Merle, O.: Estimation of magma depth for resurgent domes: An experimental approach, *Earth*
420 *Planet. Sc. Lett.*, 412, 143–151, <https://doi.org/10.1016/j.epsl.2014.12.011>, 2015.

421 Calcagno, P., Evanno, G., Trumpy, E., Carlos Gutiérrez-Negrín, L., Macías, J.L., Carrasco-Núñez, G., and Liotta, D.:
422 Preliminary 3-D geological models of Los Humeros and Aocolulco geothermal fields (Mexico)-H2020 GEMex Project,
423 *Adv. Geosci.*, 45, 321–333, <https://doi.org/10.5194/adgeo-45-321-2018>, 2018.

424 Carlino, S.: The process of resurgence for Ischia Island (southern Italy) since 55 ka: The laccolith model and
425 implications for eruption forecasting, *B. Volcanol.*, 74, 947–961. <https://doi.org/10.1007/s00445-012-0578-0>, 2012.

426 Carrasco-Núñez, G., and Branney, M.J.: Progressive assembly of a massive layer of ignimbrite with a normal-to-reverse
427 compositional zoning: The Zaragoza ignimbrite of central Mexico, *B. Volcanol.*, 68, 3–20,
428 <https://doi.org/10.1007/s00445-005-0416-8>, 2005.

429 Carrasco-Núñez, G., McCurry, M., Branney, M.J., Norry, M., and Willcox, C.: Complex magma mixing, mingling, and
430 withdrawal associated with an intra-Plinian ignimbrite eruption at a large silicic caldera volcano: Los Humeros of
431 central Mexico, *Bull. Geol. Soc. Am.*, 124, 1793–1809, <https://doi.org/10.1130/B30501.1>, 2012.

432 Carrasco-Núñez, G., López-Martínez, M., Hernández, J., and Vargas, V.: Subsurface stratigraphy and its correlation
433 with the surficial geology at Los Humeros geothermal field, eastern Trans-Mexican Volcanic Belt, *Geothermics*, 67, 1–
434 17, <https://doi.org/10.1016/j.geothermics.2017.01.001>, 2017a.

435 Carrasco-Núñez, G., Hernández, J., De León, L., Dávila, P., Norini, G., Bernal, J.P., Jicha, B., Navarro, M., López-
436 Quiroz, P., and Digitalis, T.: Geologic Map of Los Humeros volcanic complex and geothermal field, eastern Trans-
437 Mexican Volcanic Belt, *Terra Digitalis*, 1, 1–11, <https://doi.org/10.22201/igg.terradigitalis.2017.2.24.78>, 2017b.

438 Carrasco-Núñez, G., Bernal, J.P., Dávila, P., Jicha, B., Giordano, G., and Hernández, J.: Reappraisal of Los Humeros
439 volcanic complex by new U/Th zircon and ⁴⁰Ar/³⁹Ar dating: Implications for greater geothermal potential, *Geochem.*
440 *Geophys. Geosy.*, 19, 132-149, <https://doi.org/10.1002/2017GC007044>, 2018.

441 Catalano, S., De Guidi, G., Lanzafame, G., Monaco, C., and Tortotici, L.: Late quaternary deformation on the island on
442 Pantelleria: new constraints for the recent tectonic evolution of the Sicily Channel Rift (southern Italy). *J. Geodyn.* 48,
443 75–82, 2009.

444 Chang, W.L., Smith, R.B., Wicks, C., Farrell, J.M., and Puskas, C.M.: Accelerated uplift and magmatic intrusion of the
445 Yellowstone Caldera, 2004 to 2006, *Science*, 318, 952-956, <https://doi.org/10.1126/science.1146842>, 2007.

446 Christiansen, R.L., Lipman, P.W., Carr, W.J., Byers, F.M., Orkild, P.P., and Sargent, K.A.: Timber Mountain-Oasis
447 Valley caldera complex of southern Nevada, *Geol. Soc. Am. Bull.*, 88, 943-959, [https://doi.org/10.1130/0016-7606\(1977\)88<943:TMVCCO>2.0.CO;2](https://doi.org/10.1130/0016-7606(1977)88<943:TMVCCO>2.0.CO;2), 1977.

448 Dávila-Harris, P., and Carrasco-Núñez, G.: An unusual syn-eruptive bimodal eruption: The Holocene Cuicuiltic
449 Member at Los Humeros caldera, Mexico, *J. Volcanol. Geoth. Res.*, 271, 24–42,
450 <https://doi.org/10.1016/j.jvolgeores.2013.11.020>, 2014.

451 de Silva, S.L., Mucek, A.E., Gregg, P.M., and Pratomo, I.: Resurgent Toba - field, chronologic, and model constraints
452 on time scales and mechanisms of resurgence at large calderas, *Front. Earth Sci.*, 3, 1–17,
453 <https://doi.org/10.3389/feart.2015.00025>, 2015.

454 Doblas, M.: Slickenside kinematic indicators, *Tectonophysics*, 295, 187–197, [https://doi.org/10.1016/S0040-1951\(98\)00120-6](https://doi.org/10.1016/S0040-1951(98)00120-6), 1998.

455 Du Bray, E.A., and Pallister, J.S.: Recrystallization and anatexis along the plutonic–volcanic contact of the Turkey
456 Creek caldera, Arizona, *Geol. Soc. Am. Bull.*, 111, 143–153, [https://doi.org/10.1130/0016-7606\(1999\)111<0143:RAAATP>2.3.CO;2](https://doi.org/10.1130/0016-7606(1999)111<0143:RAAATP>2.3.CO;2), 1999.

457 Elston, W.: Mid-Tertiary ash flow tuff cauldrons, southwestern New Mexico, *J. Geophys. Res.*, 89, 8733–8750,
458 <https://doi.org/10.1029/JB089iB10p08733>, 1984.

459 Evans, K.F., Zappone, A., Kraft, T., Deichmann, N., and Moia, F.: A survey of the induced seismic responses to fluid
460 injection in geothermal and CO₂ reservoirs in Europe, *Geothermics*, 41, 30-54,
461 <https://doi.org/10.1016/j.geothermics.2011.08.002>, 2012.

462 Ferrari, L., Orozco-Esquivel, T., Manea, V., and Manea, M.: The dynamic history of the Trans-Mexican Volcanic Belt
463 and the Mexico subduction zone, *Tectonophysics*, 522–523, 122–149, <https://doi.org/10.1016/j.tecto.2011.09.018>, 2012.

464 Ferriz, H., and Mahood, G.A.: Eruption Rates and Compositional Trends at Los Humeros Volcanic Center, Puebla,
465 Mexico, *J. Geophys. Res.*, 89, 8511-8524, <https://doi.org/10.1029/JB089iB10p08511>, 1984.

466 Folkes, C.B., Wright, H.M., R.A.F. Cas, de Silva, S.L., Lesti, C., and Viramonte, J.G.: A re-appraisal of the stratigraphy
467 and volcanology of the Cerro Galán volcanic system, NW Argentina, *B. Volcanol.*, 73, 1427–1454,
468 <https://doi.org/10.1007/s00445-011-0459-y>, 2011.

469 Fridrich, C.J., Smith, R.P., DeWitt, E., McKee, E.H.: Structural, eruptive, and intrusive evolution of the Grizzly Peak
470 caldera, Sawatch Range, Colorado, *Geol. Soc. Am. Bull.*, 103, 1160-1177, [https://doi.org/10.1130/0016-7606\(1991\)103<1160:SEAIEO>2.3.CO;2](https://doi.org/10.1130/0016-7606(1991)103<1160:SEAIEO>2.3.CO;2), 1991.

475 Galetto, F., Acocella, V., and Caricchi, L.: Caldera resurgence driven by magma viscosity contrasts, *Nat. Commun.*, 8,
476 1–11, <https://doi.org/10.1038/s41467-017-01632-y>, 2017.

477 Galetto, F., Bagnardi, M., Acocella, V., and Hooper, A.: Nonruptive unrest at the caldera of Alcedo Volcano (Galápagos
478 Islands) revealed by InSAR data and geodetic modelling, *J. Geophys. Res.*, 124, 3365–3381,
479 <https://doi.org/10.1029/2018JB017103>, 2019.

480 Galland, O.: Experimental modelling of ground deformation associated with shallow magma intrusions, *Earth Planet.
481 Sc. Lett.*, 317-318, 145-156, <https://doi.org/10.1016/j.epsl.2011.10.017>, 2012.

482 Galland, O., Planke, S., Ragnhild Neumann, E., and Malthe-Sørenssen, A.: Experimental modelling of shallow magma
483 emplacement: Application to saucer-shaped intrusions, *Earth Planet. Sc. Lett.*, 277, 373-383,
484 <https://doi.org/10.1016/j.epsl.2008.11.003>, 2009.

485 Goto, Y., and McPhie, J.: Tectonics, structure, and resurgence of the largest Quaternary caldera in Japan: Kutcharo,
486 Hokkaido, *Geol. Soc. Am. Bull.*, 130, 1307-1322, <https://doi.org/10.1130/B31900.1>, 2018.

487 Guillou-Frottier, L., Burov, E.B., and Milési, J.P.: Genetic links between ash-flow calderas and associated ore deposits
488 as revealed by large-scale thermo-mechanical modelling, *J. Volcanol. Geoth. Res.*, 102, 339–361,
489 [https://doi.org/10.1016/S0377-0273\(00\)00246-8](https://doi.org/10.1016/S0377-0273(00)00246-8), 2000.

490 Hildreth, W., Fierstein, J., and Calvert, A.: Early postcaldera rhyolite and structural resurgence at Long Valley
491 Caldera, California, *J. Volcanol. Geoth. Res.*, 335, 1-34, <http://dx.doi.org/10.1016/j.jvolgeores.2017.01.005>, 2017.

492 Kennedy, B., Wilcock, J., and Stix, J.: Caldera resurgence during magma replenishment and rejuvenation at Valles and
493 Lake City calderas, *B. Volcanol.*, 74, 1833–1847, <https://doi.org/10.1007/s00445-012-0641-x>, 2012.

494 Lipman, P. W.: The roots of ash flow calderas in Western North America: windows into the tops of granitic batholiths, *J.
495 Geophys. Res.*, 89, 8801–8841, <https://doi.org/10.1029/JB089iB10p08801>, 1984.

496 Lermo, J., Lorenzo, C., Jiménez, N., Ramos, E., Ângulo, J., Israel, J., Téllez, N., Machado, O., Álvarez, I., Torres, R.,
497 Alfaro R.: Analisis de la actividad sismica (1994-2016), su relacion con los pozos inyectoros y productores y aplicación
498 de nuevas tecnicas geofisica para caracterizar las zonas anómalas del campo geotérmico de Los Humeros, CEMIE-
499 GEO, Mexico, Internal Rep., 42 pp., 2018.

500 Lucci, F., Carrasco-Núñez, G., Rossetti, F., Theye, T., White, J. C., Urbani, S., Azizi, H., Asahara, Y., and Giordano, G.:
501 Anatomy of the magmatic plumbing system of Los Humeros Caldera (Mexico): implications for geothermal systems,
502 *Solid Earth Discuss.*, <https://doi.org/10.5194/se-2019-86>, in review, 2019.

503 Marsh, B.D.: On the mechanics of caldera resurgence, *J. Geophys. Res.*, 89, 8245–8251,
504 <https://doi.org/10.1029/JB089iB10p08245>, 1984.

505 Martí, J., Ablay, G.J., Redshaw, L.T., and Sparks, R.S.J.: Experimental studies of collapse calderas, *J. Geol. Soc.
506 London*, 151, 919-929, <https://doi.org/10.1144/gsjgs.151.6.0919>, 1994.

507 Merle, O., Borgia, A.: Scaled experiments of volcanic spreading, *J. Geophys. Res.*, 101, 13805-13817,
508 <https://doi.org/10.1029/95JB03736>, 1996.

509 Morán-Zenteno, D.J., Alba-Aldave, L.A., Solé, J., and Iriondo, A.: A major resurgent caldera in southern Mexico: the
510 source of the late Eocene Tlzapotla ignimbrite. *J. Volcanol. Geoth. Res.*, 136, 97–119,
511 <https://doi.org/10.1016/j.jvolgeores.2004.04.002>, 2004.

512 Moretti, R., Troise, C., Sarno, F., and De Natale, G.: Caldera unrest driven by CO₂ induced drying of the deep
513 hydrothermal system, *Sci. Rep. UK*, 8, <https://doi.org/10.1038/s41598-018-26610-2>, 2018.

514 Mueller, W.U., Stix, J., Corcoran, P.L., Daigneault, R.: Subaqueous calderas in the Archean Abitibi greenstone belt: An
515 overview and new ideas, *Ore Geol. Rev.*, 35, 4–46, <https://doi.org/10.1016/j.oregeorev.2008.12.003>, 2009.

516 Norini, G., Groppelli, G., Sulpizio, R., Carrasco-Núñez, G., Dávila-Harris, P., Pelliccioli, C., Zucca, F., and De Franco,
517 R.: Structural analysis and thermal remote sensing of the Los Humeros Volcanic Complex: Implications for volcano
518 structure and geothermal exploration, *J. Volcanol. Geoth. Res.*, 301, 221–237,
519 <https://doi.org/10.1016/j.jvolgeores.2015.05.014>, 2015.

520 Norini, G., Carrasco-Núñez, G., Corbo-Camargo, F., Lermo, J., Hernández Rojas, J., Castro, C., Bonini, M., Montanari,
521 D., Corti, G., Moratti, G., Chavez, G., Ramirez, M., and Cedillo F.: The structural architecture of the Los Humeros
522 volcanic complex and geothermal field, *J. Volcanol. Geoth. Res.*, 381, 312–329.
523 <https://doi.org/10.1016/j.jvolgeores.2019.06.010>, 2019.

524 Matsumoto, A., and Nakagawa, M.: Formation and evolution of silicic magma plumbing system: Petrology of the
525 volcanic rocks of Usu volcano, Hokkaido, Japan, *J. Volcanol. Geoth. Res.*, 196, 185–207,
526 <https://doi.org/10.1016/j.jvolgeores.2010.07.014>, 2010.

527 Pribnow, D.F.C., Schütze, C., Hurter, S.J., Flechsig, C., Sass, J.H.: Fluid flow in the resurgent dome of Long Valley
528 Caldera: Implications from thermal data and deep electrical sounding. *J. Volcanol. Geoth. Res.*, 127, 329–345,
529 [https://doi.org/10.1016/S0377-0273\(03\)00175-6](https://doi.org/10.1016/S0377-0273(03)00175-6), 2003.

530 Roche, O., Druitt, T.H., and Merle, O.: Experimental study of caldera formation, *J. Geophys. Res.*, 105,
531 <https://doi.org/10.1029/1999JB900298>, 395–416, 2000.

532 Smith, R. L., and Bailey, R. A.: Resurgent cauldrons, *Geol. Soc. Am. Mem.*, 116, 613–662,
533 <https://doi.org/10.1130/MEM116>, 1968.

534 Stix, J., Kennedy, B., Hannington, M., Gibson, H., Fiske, R., Mueller, W., Franklin, J.: Caldera-forming processes and
535 the origin of submarine volcanogenic massive sulfide deposits, *Geology*, 31, 375–378, [https://doi.org/10.1130/0091-](https://doi.org/10.1130/0091-7613(2003)031<0375:CFPATO>2.0.CO;2)
536 [7613\(2003\)031<0375:CFPATO>2.0.CO;2](https://doi.org/10.1130/0091-7613(2003)031<0375:CFPATO>2.0.CO;2), 2003.

537 Swanson, E., and McDowell, F.: Geology and geochronology of the Tomochoic caldera, Chihuahua, Mexico, *Geol. Soc.*
538 *Am. Bull.*, 96, 1477–1482, [https://doi.org/10.1130/0016-7606\(1985\)96<1477:GAGOTT>2.0.CO;2](https://doi.org/10.1130/0016-7606(1985)96<1477:GAGOTT>2.0.CO;2), 1985.

539 Tomiya, A., Takahashi, E., Furukawa, N., Suzuki, T.: Depth and evolution of a silicic magma chamber: Melting
540 experiments on a low-K rhyolite from Usu volcano, Japan, *J. Petrol.*, 51, 1333–1354,
541 <https://doi.org/10.1093/petrology/egg021>, 2010.

542 Ueda, H., Nagai, M., and Tanada, T.: Phreatic eruptions and deformation of Ioto Island (Iwo-jima), Japan, triggered by
543 deep magma injection, *Earth Planets Space*, 70, <https://doi.org/10.1186/s40623-018-0811-y>, 2018.

544 Verma, M.P., Verma, S.P., and Sanvicente, H.: Temperature field simulation with stratification model of magma
545 chamber under Los Humeros caldera, Puebla, Mexico, *Geothermics*, 19, 187–197, [https://doi.org/10.1016/0375-](https://doi.org/10.1016/0375-6505(90)90015-4)
546 [6505\(90\)90015-4](https://doi.org/10.1016/0375-6505(90)90015-4), 1990.

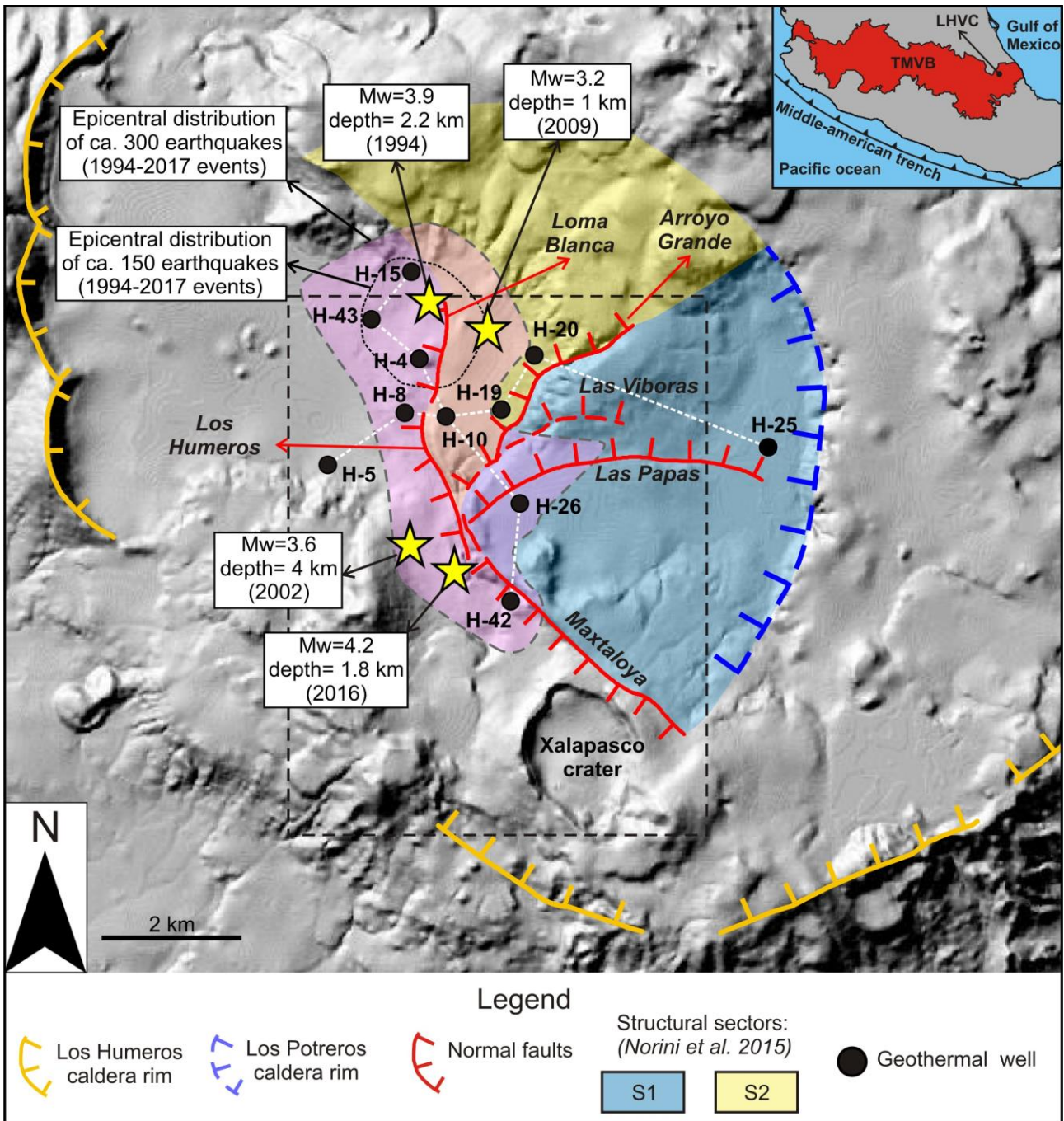
547 Verma, S.P., Gómez-Arias, E., and Andaverde, J.: Thermal sensitivity analysis of emplacement of the magma chamber
548 in Los Humeros caldera, Puebla, Mexico, *Int. Geol. Rev.*, 53, 905–925, <https://doi.org/10.1080/00206810903234296>,
549 2011.

550 Verma, S.P.: Magma genesis and chamber processes at Los Humeros caldera, Mexico - Nd and Sr isotope data, *Nature*,
551 302, 52–55, <https://doi.org/10.1038/302052a0>, 1983.

552 Verma, S.P.: Geochemical evidence for a lithospheric source for magmas from Los Humeros caldera, Puebla, Mexico.
553 *Chem. Geol.* 164, 35–60, [https://doi.org/10.1016/S0009-2541\(99\)00138-2](https://doi.org/10.1016/S0009-2541(99)00138-2), 2000.

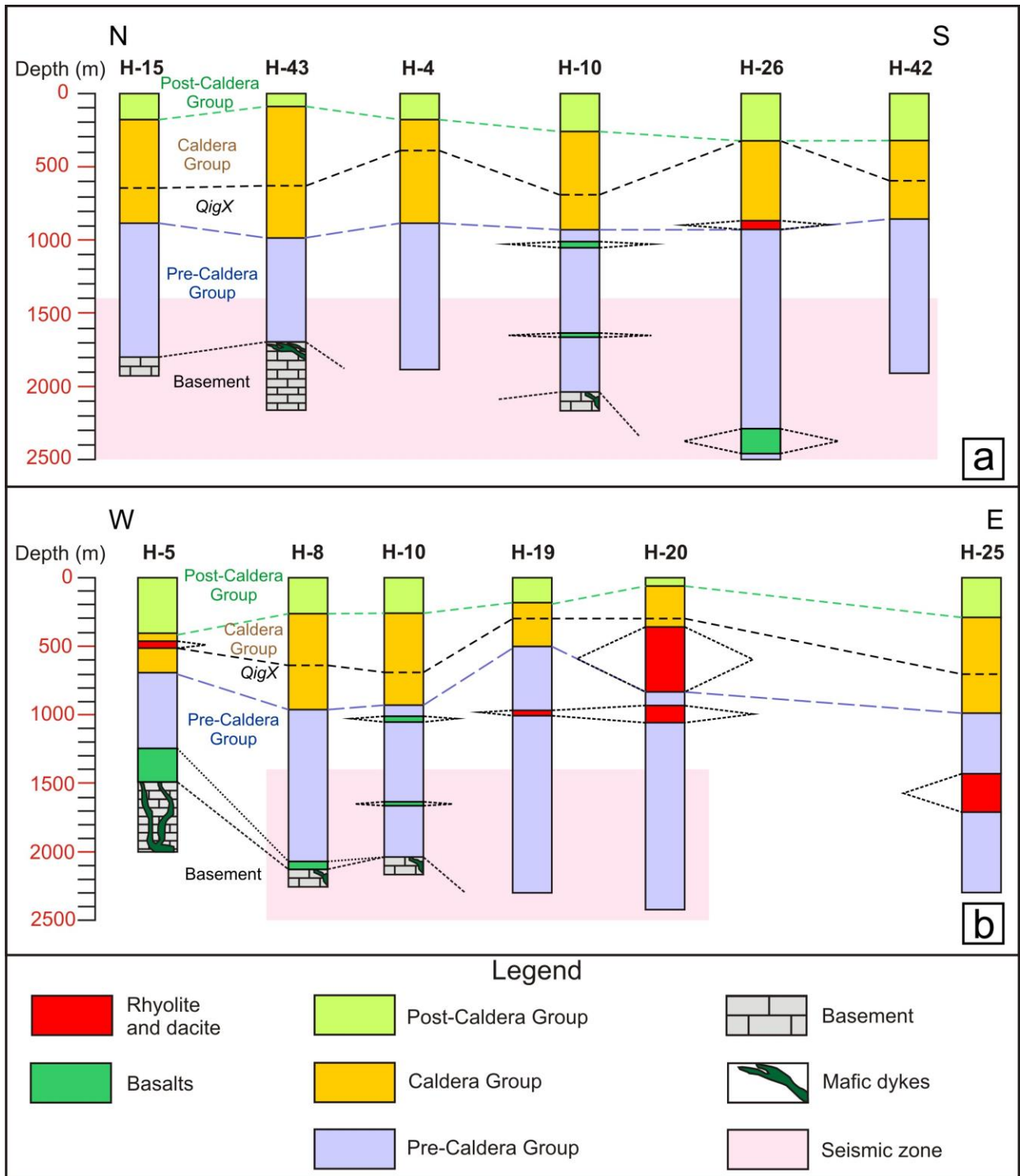
554 Walter, T.R., and Troll, V.R.: Formation of caldera periphery faults: an experimental study, *B. Volcanol.*, 63, 191–203,
555 <https://doi.org/10.1007/s004450100135>, 2001.

556 Walter, T.R., Wang, R., Acocella, V., Neri, M., Grosser, H., and Zschau, J: Simultaneous magma and gas eruptions at three
557 volcanoes in southern Italy: an earthquake trigger ?, *Geology*, 37, 251–254, <https://doi.org/10.1130/G25396A>, 2009.
558 Wilcox, C.P.: Eruptive, magmatic and structural evolution of a large explosive caldera volcano, Los Humeros, Central
559 Mexico, Ph.D. thesis, Department of Geology, University of Leicester, United Kingdom, 317 pp., 2011.



560
 561 **Figure 1:** Shaded relief image (illuminated from the NE) obtained from 15 m resolution DEM of the Los Humeros Volcanic
 562 Complex (LHVC) showing the main structural features (faults and caldera rim, modified from Norini et al. (2015); Calcagno
 563 et al. (2018) and some geothermal wells referred in the text and in Figures 2a-b. The white dashed lines indicate the direction
 564 of the correlation sections shown in Figures 2a-b. The black rectangle indicates the studied area within the Los Potreros
 565 Caldera shown in Figure 4. The Inset box show the location of the LHVC (black dot and arrow) within the eastern sector of
 566 the Trans Mexican Volcanic Belt (TMVB). The structural sectors S1 and S2 correspond to the resurgent block inferred by
 567 Norini et al. (2015). Seismicity data from Lermo et al. (2018).

568
 569
 570
 571
 572



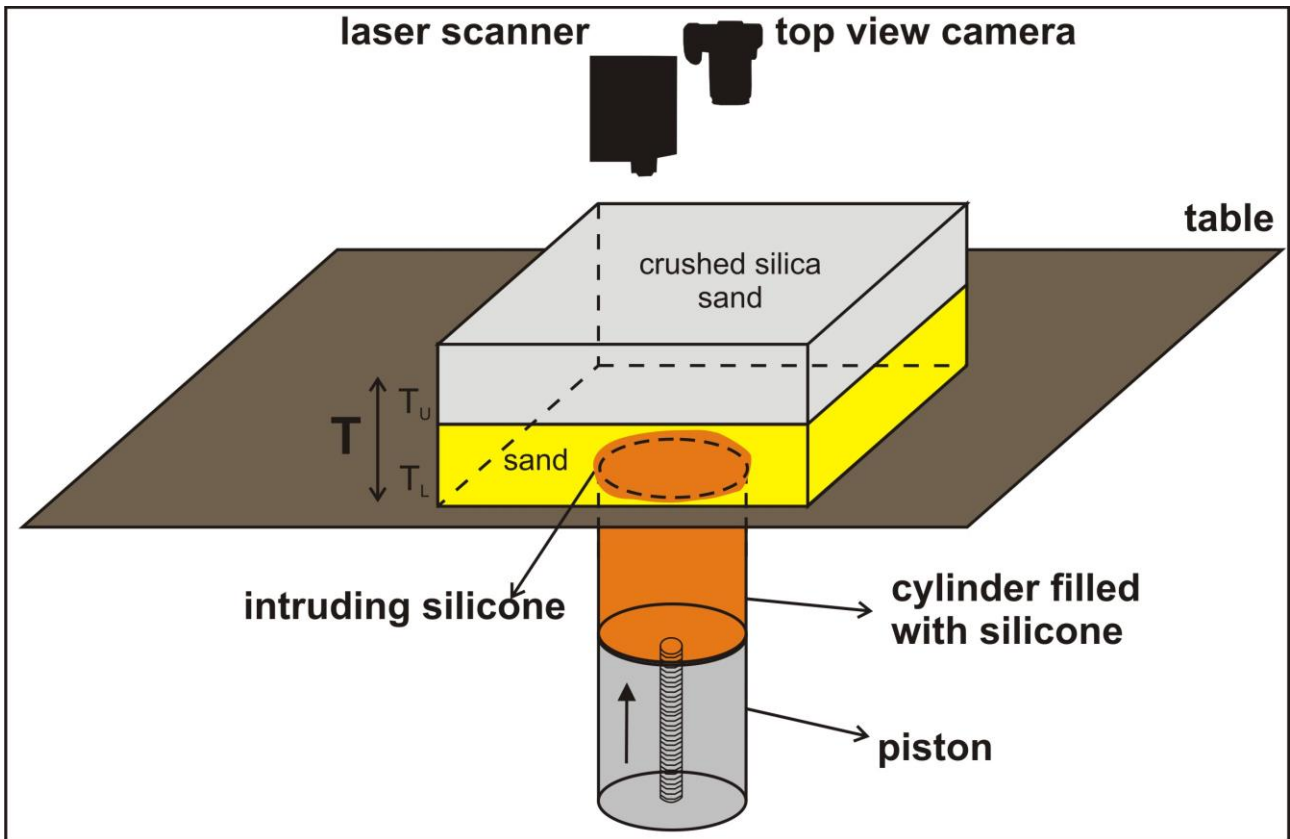
573

574

575

576

Figure 2: In depth correlation of lithostratigraphic units along the N-S (a) and W-E (b) direction (redrawn after Carrasco-Núñez et al. (2017a) and Arellano et al. (2003). Depth:horizontal distance=1:1. Location of the correlation line is shown in Figure 1. QigX= Xaltipan ignimbrite.



577

578

579

580

581

582

583

584

585

586

587

588

589

590

591

592

593

594

595

596

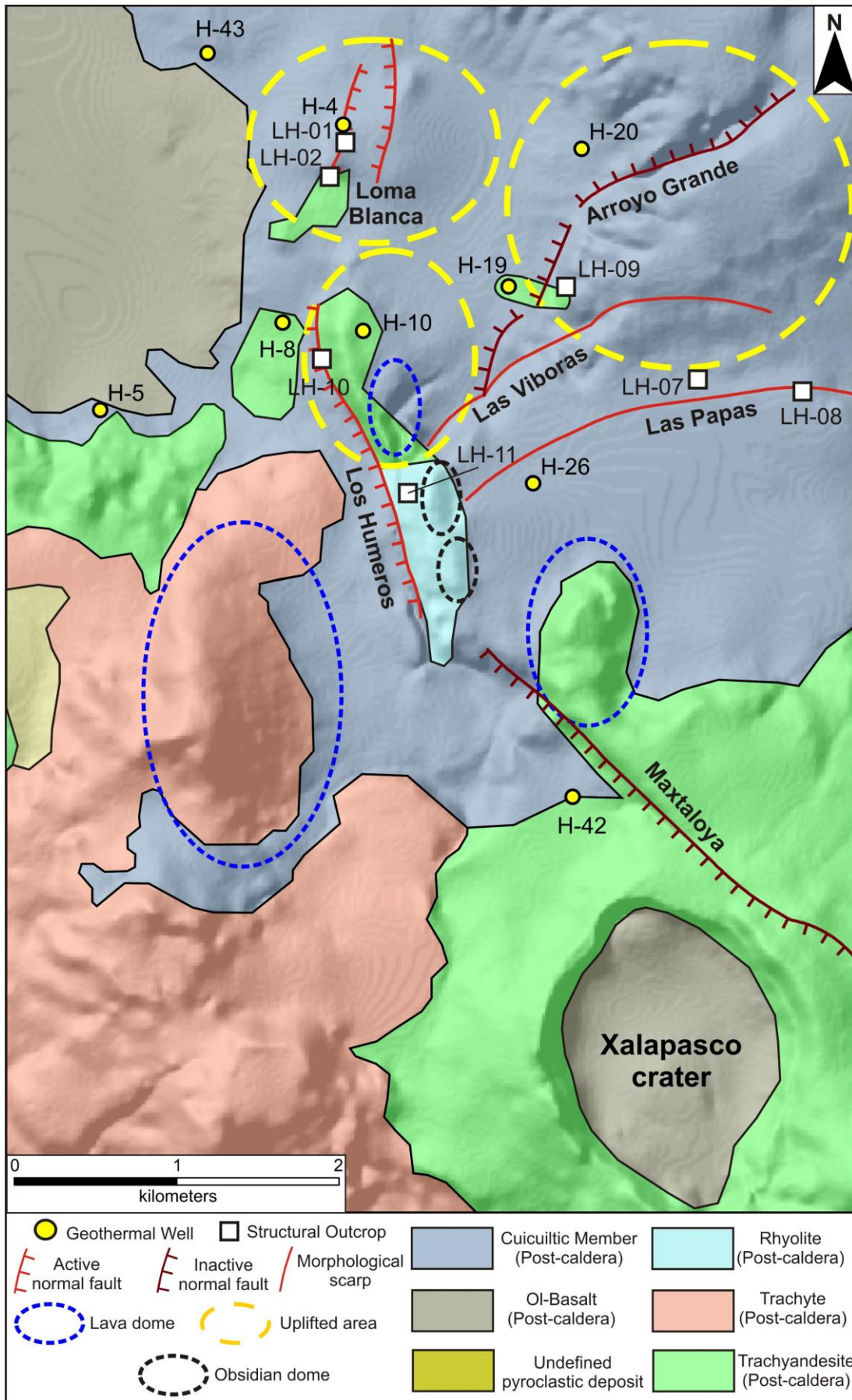
597

598

599

600

Figure 3: Experimental set-up. A motor controlled piston pushes upward the silicone at a fixed rate (2mm/hr) from the base of the layered sand pack (the diameter of the silicone is 8 cm). A laser scanner and a camera record the surface deformation induced by the intruding silicone. T = total overburden thickness. T_U = upper layer thickness, T_L = lower layer thickness.

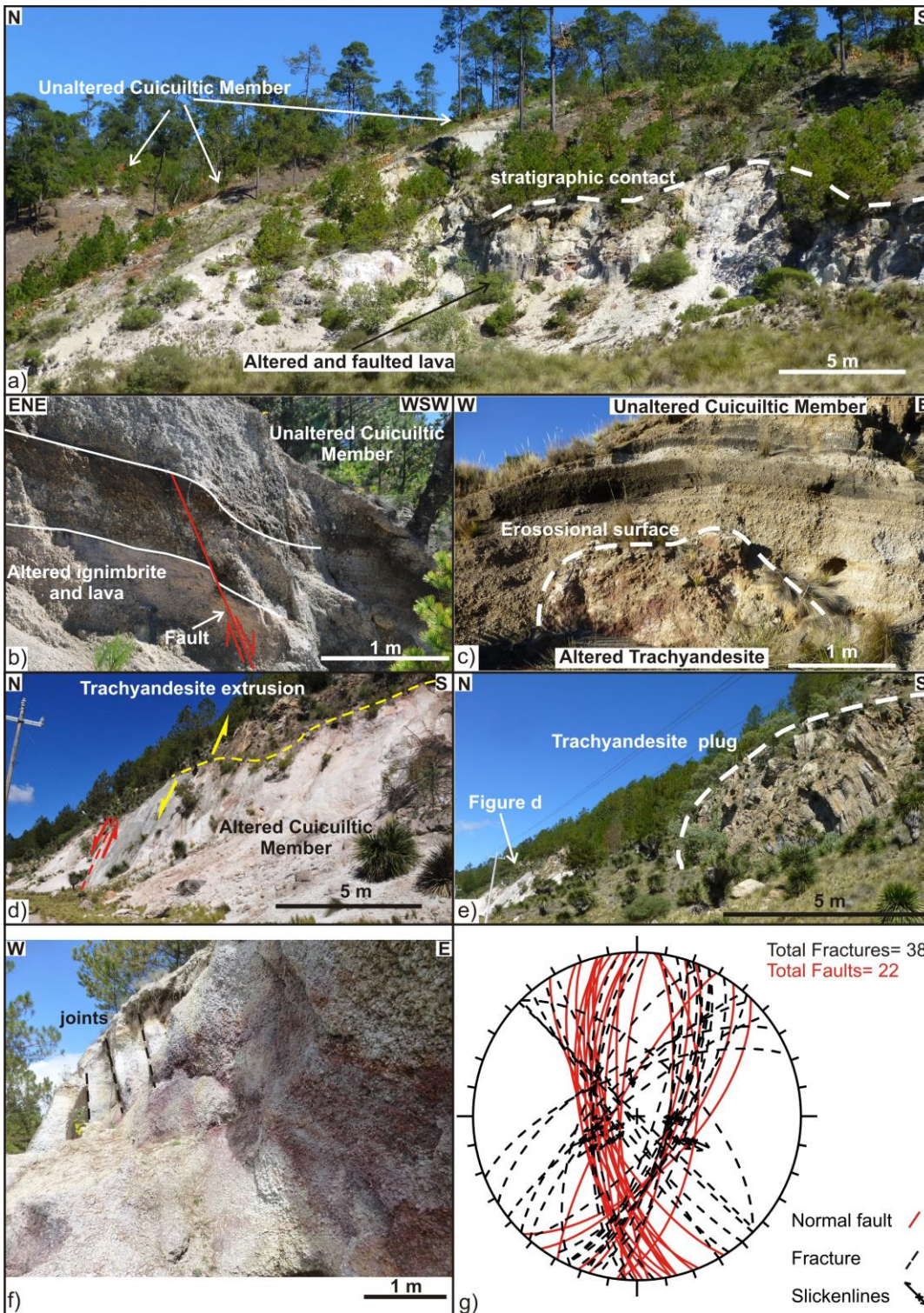


601
602
603

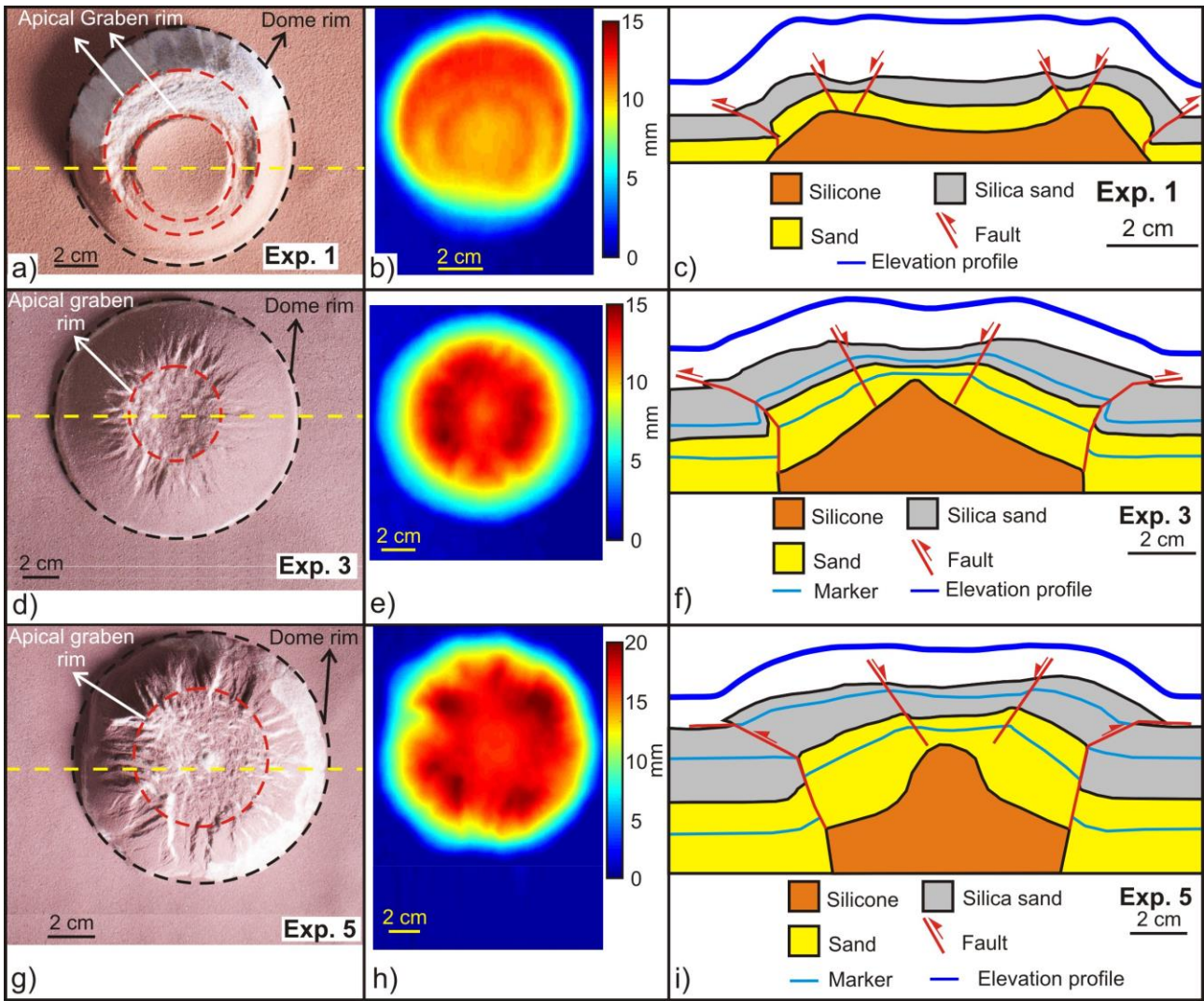
Figure 4: Simplified geological structural map of the studied area; reinterpreted after (Norini et al., 2015; Carrasco- Núñez et al., 2017b; Calcagno et al., 2018).



604
 605 **Figure 5: a) Panoramic view from Xalapasco crater (looking towards N) of the lava domes aligned N-S. b) Unaltered**
 606 **Cuicuiltic Member (LH-07). c) Unaltered Cuicuiltic Member covering a layered pyroclastic deposit, which can be laterally**
 607 **correlated with the Xoxoctic Tuff (LH-08). The erosional surface preceding the deposition of the Cuicuiltic Member is shown**
 608 **(dashed white line).**

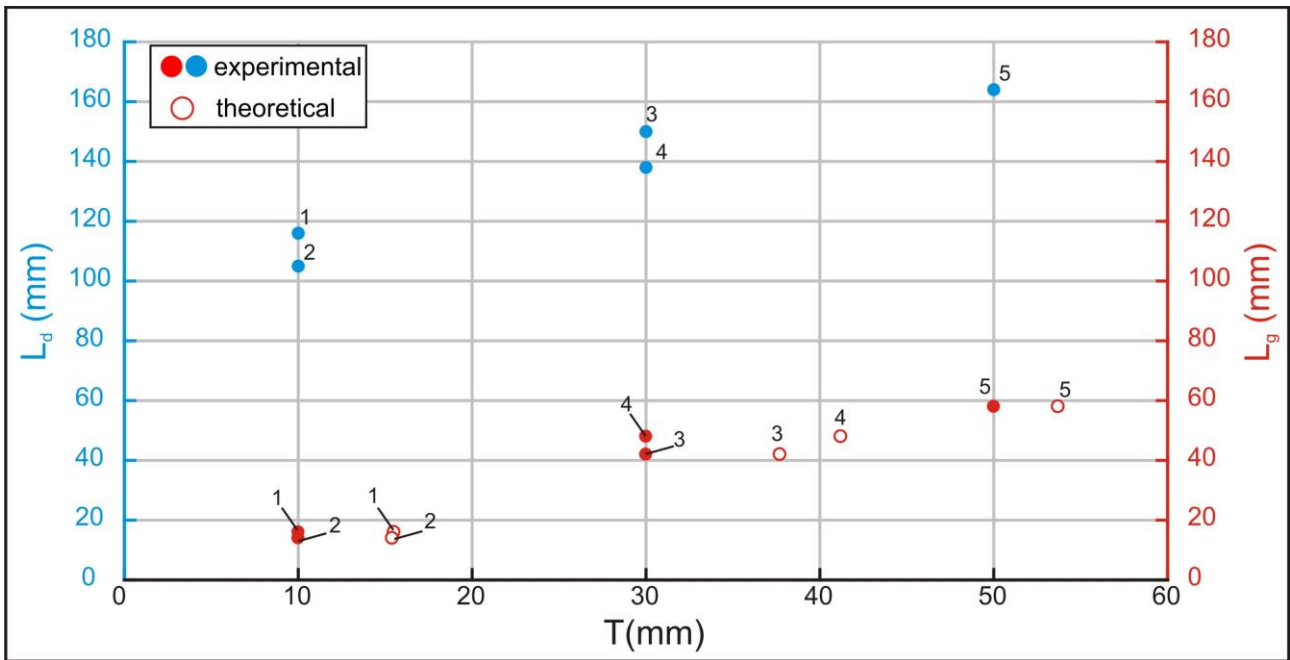


609
 610 **Figure 6:** a) Panoramic view of the Arroyo Grande fault scarp showing the unaltered Cuicuiltic Member covering the altered
 611 and faulted ignimbrite and lavas (site LH-09). b) Normal fault affecting the altered ignimbrite deposits unconformably
 612 covered by the post-caldera, unaltered Cuicuiltic Member deposits (LH-09). Note that the Cuicuiltic Member deposits are
 613 not faulted at this location; the fault can be thus considered as a fossil fault with respect to the Cuicuiltic Member deposition.
 614 c) Block of altered trachyandesite buried by unaltered Cuicuiltic Member layers along the Maxtaloya fault scarp. d) Los
 615 Humeros fault scarp (LH-10) induced by the ascent of the trachyandesitic extrusion on top of the fault plane. e)
 616 Trachyandesite plug cropping out ~150 southward the fault scarp shown in d) (indicated by the red arrow). f) Jointing and
 617 alteration of the Cuicuiltic Member within the apical depression of the Loma Blanca dome (LH-01). e) Equal-area stereo-plot
 618 of the attitudes of faults and fractures in all the structural outcrops.



619
620
621
622
623
624
625
626
627
628
629
630
631
632
633
634
635
636
637

Figure 7: a) d) g) Top view image of the experiments 1, 3 and 5. b) e) h) cumulative vertical displacement; colour scale is proportional to the amount of uplift. c) f) i) Drawing of the cross section view obtained after cutting the section close to the dome center. The elevation profiles are obtained from laser scanner data. The yellow dashed line in a) d) g) indicates the trace of the section views and of the elevation profiles.

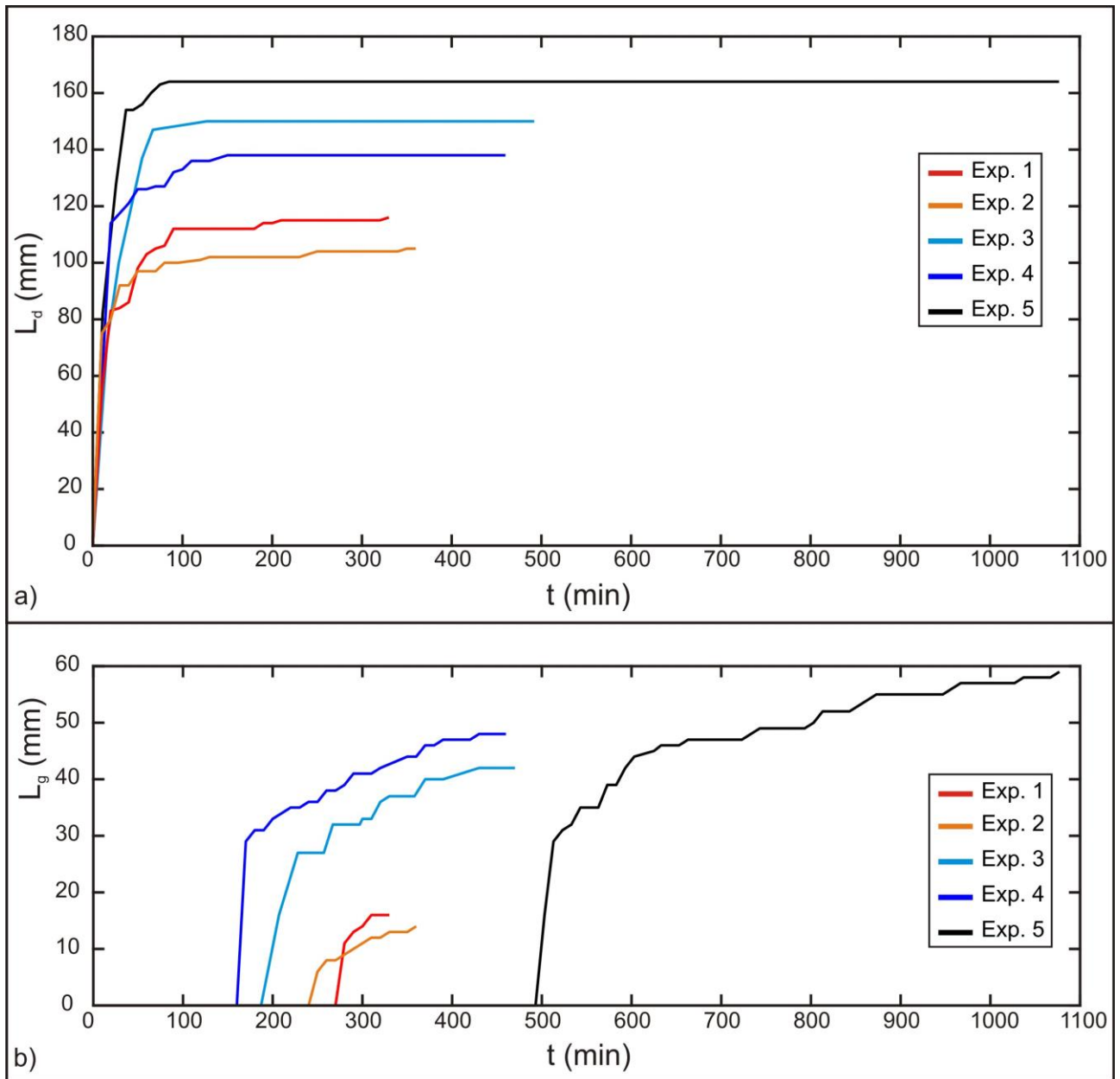


638

639

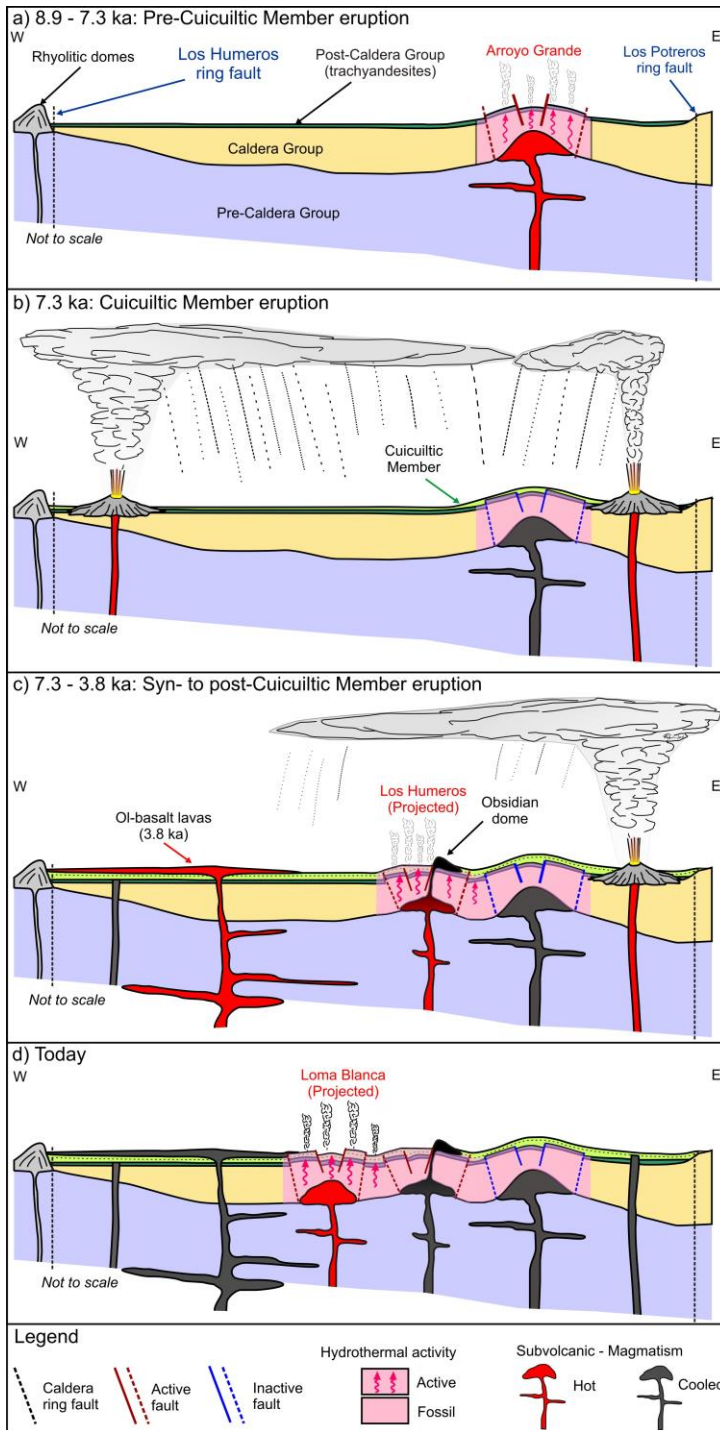
640

Figure 8: L_g (apical depression width) and L_d (dome diameter) versus T (overburden thickness). Theoretical values calculated after equation 1 (see discussion section). The numbers above each point indicate the experiment number.



641
 642 **Figure 9: a) Time evolution of the dome diameter (L_d). b) Time evolution of the apical depression width (L_g). Both L_d and L_g**
 643 **show a similar evolution trend with a first stage of abrupt increase at the beginning of each experiment. In the second stage**
 644 **L_d becomes constant at $t \sim 90$ min (experiments 1-2-3), $t \sim 150$ min (experiment 4) and $t \sim 65$ min (experiment 5) while L_g**
 645 **increases slightly from $t \sim 250$ -280 min (experiments 1-2), $t \sim 210$ min and ~ 170 min (experiments 3 and 4) and $t \sim 530$ min**
 646 **(experiment 5) till the end of the experiment.**

647
 648
 649
 650
 651
 652
 653
 654
 655
 656



657

658

659

660

661

662

663

664

665

666

667

668

Figure 10: Schematic model of the evolution of the sub-surface structure of the Los Potreros caldera floor. Multiple magmatic intrusions located at relatively shallow depth (< 1 km) are responsible for the localized bulging of the caldera floor (Loma Blanca, Los Humeros and Arroyo Grande uplifted areas). a) Pre Cuicuiltic Member eruption: emplacement of a felsic intrusion at shallow depth and formation of the Arroyo grande bulge characterized by extensional faulting at its top, reverse faulting at its base and hydrothermalism. b) Cuicuiltic Member eruption: eruption of the Cuicuiltic Member covering the hydrothermally altered post-caldera trachyandesitic lavas. c) Syn to post Cuicuiltic Member eruption: formation of the Los Humeros fault and extrusion of obsidian lava domes along the fault scarp. As the trachyandesitic domes are covered with Cuicuiltic Member only at his base, the lava extrusion occurred during and post the Cuicuiltic Member eruption. d) Formation of the Loma Blanca bulge with the current hydrothermal activity and extensional faulting occurring within the apical depression. Notice that the emplacement of the successive most recent domes (Los Humeros and Loma blanca) are not aligned on the same plane, they are shown for practical purposes.

Stage	Age (ka)	Main stratigraphic units
Post-caldera	< 69	Cuicuiltic Member and trachyandesitic to basaltic lavas
		Llano Tuff
		Xoxoctic Tuff
		Rhyolitic domes
Caldera	164-69	Zaragoza ignimbrite
		Faby Tuff
		Xaltipan ignimbrite
Pre-Caldera	700-164	Rhyolitic Domes

669 Table 1 Summary of the main stratigraphic units of the three evolutionary stages of the Los Humeros Volcanic complex
670 (Carrasco-Núñez et al., 2017b, 2018).

Parameter	Definition	Value (experiments)	Value (nature)
T	Thickness of the overburden	1-5 X 10 ⁻² m	300-2000 m
L _d	Dome diameter	1-1.6 X 10 ⁻¹ m	2000 m
H	Dome height	1.1-2 X 10 ⁻² m	100 m
ρ _s	Density of brittle overburden	1400 kg/m ³	2800 kg/m ³
φ	Angle of internal friction	35°	25-40°
τ ₀	Cohesion (brittle overburden)	300 Pa	10 ⁶ Pa
ρ _m	Density of intrusive material	1000 kg/m ³	2500 kg/m ³
μ _m	Viscosity of intrusive material	10 ⁴ Pa s	10 ¹⁵ Pa s
g	Gravity	9.8 m/s ²	9.8 m/s ²
t	Timespan for deformation	2.8-6.5 X 10 ⁴ s	1.9 X 10 ¹² s

671 Table 2. Comparison of the geometric and material properties parameters of the experiments and nature.

Dimensionless ratio	Experiments	Nature
Π ₁ = T/L _d	0.1-0.5	0.15-1
Π ₂ = H/L _d	0.08-0.2	0.05-0.1
Π ₃ = ρ _s /ρ _m	1.4	1.12
Π ₄ = φ	35	25-40
Π ₅ = ρ _m H ² /μ _{mt}	6.1 X 10 ⁻¹⁰	1.3 X 10 ⁻²⁰
Π ₆ = ρ _m gHt/μ _m	1.3 X 10 ³	4.6 X 10 ³
Π ₇ = ρ _s gT/τ ₀	2.3	8.24

672 Table 3. Definition and values of the dimensionless ratios Π in nature and in the experiments.

Exp	T (mm)	L _g (mm)	L _d (mm)	θ	α	T _t (mm)	σ (%)
1	10	16	116	58°	14°	15.5	55
2	10	14	105	63°	27°	15.4	54
3	30	42	150	58°	14°	37.7	27
4	30	48	138	56°	18°	41.2	37
5	50	58	164	58°	21°	53.7	7

673 Table 4. Measured (L_g, L_d, θ, α) and imposed (T) parameters in the experiments. T=overburden thickness; L_d= dome
674 diameter; L_g= apical depression width; θ= apical depression fault dip; α= dome flank mean dip; T_t= theoretical overburden

675 thickness calculated with equation 1 (Brothelände and Merle, 2015, see discussion section); σ = percentage difference between
676 T and T_c .